Case Study of a Hailstorm in Colorado. Part III: Airflow From Triple-Doppler Measurements

G. BRANT FOOTE AND HAROLD W. FRANK

Convective Storms Division, National Center for Atmospheric Research,[1] Boulder, CO 80307

(Manuscript received 19 August 1982, in final form 26 October 1982)

ABSTRACT

Triple-Doppler measurements are presented for a hailstorm of moderate intensity that occurred over the High Plains of northeastern Colorado, and an airflow model is synthesized. The storm had a number of persistent features similar to previous descriptions of supercells. However, its evolution is shown to be intermediate in a certain sense between classical multicell and supercell models. A new model based on the Doppler observations, termed "weak evolution," emphasizes gradual changes in the structure of a long-lived updraft. The new airflow model explains the periodic echo intensifications noted for this storm, and seems to apply well to other storms discussed in the literature.

1. Introduction

This paper examines the air motion in a moderate hailstorm observed on 22 July 1976 as part of the National Hail Research Experiment (NHRE). The storm passed over the small town of Westplains, and is hereafter called the Westplains storm. The data discussed here, obtained from three Doppler radars making coordinated scans, pertain only to specific periods during the last half of the storm's lifetime. In the first part of this study (Foote and Wade, 1982; hereafter referred to as Part I) the structure and evolution of the storm was described through its full lifetime in terms of conventional radar reflectivity measurements (in Part I the storm is referred to as Storm III to contrast it with others on that day). Aircraft penetrations through the middle levels of the storm, carried out in the last half of its lifetime, are discussed by Heymsfield and Musil (1982). The purpose in this paper is to synthesize a model of the airflow and its evolution based primarily on the Doppler radar measurements.

Recent studies in which thunderstorm airflow patterns have been determined from Doppler radar measurements include dual-Doppler investigations by Miller (1975), Lhermitte and Gilet (1975), Kropfli and Miller (1976), Heymsfield (1978) and Brandes (1978, 1981), a triple-Doppler study by Heymsfield (1981), and one by Ray *et al.* (1981) that employs four radars. These papers demonstrate that Doppler measurements can yield qualitatively reasonable flow patterns, but the accuracy of Doppler-derived velocity fields remains a subject of some uncertainty. The complementary data obtained in the present case provide an opportunity to compare independent air motion estimates.

In the following section we review the procedures used in this analysis and the resolution and errors involved. We then examine the storm-scale airflow pattern which, despite the moderate size and evolutionary properties of the storm (see Part I), is reminiscent of models proposed by Browning (1964) and Browning and Foote (1976) for supercell storms. Variability of the flow field and details of the internal kinematic structure are addressed using results from two time periods separated by about forty minutes, each period being represented by three consecutive Doppler scans spaced at 5–9 min intervals.

2. The nature of the data

Four Doppler radars were operated during the 1976 NHRE field season. Two X-band (3.2 cm wavelength) radars from the National Oceanic and Atmospheric Administration Wave Propagation Laboratory, termed NOAA-C and NOAA-D, were located on the north side of the experimental area, and two C-band (5.4 cm wavelength) radars from the Field Observing Facility of the National Center for Atmospheric Research, termed CP-3 and CP-4, were located on the south side as shown in Fig. 1. The four radar locations describe a parallelogram with a maximum diagonal dimension of about 70 km. Each Doppler radar scanned back and forth in an appropriate azimuth sector, beginning at an elevation angle just above the radar's horizon and incrementing the elevation angle upward between sector scans. On 22

[1] The National Center for Atmospheric Research is sponsored by the National Science Foundation.

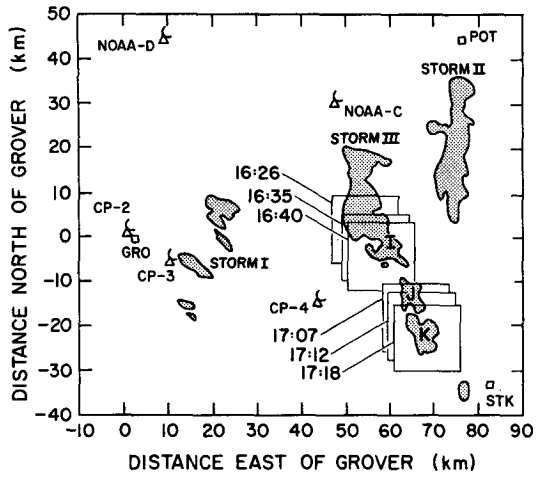

FIG. 1. Layout of the radar network relative to Storms I, II and III. Storm III is called the Westplains storm in the text. Doppler radars NOAA-C, NOAA-D and CP-3 are used for triple-Doppler analysis. Envelopes of reflectivity in excess of 55 dB(Z_e) are shown for Storm III and neighboring Storms I and II for the period 1500–1800 MDT 22 July 1976. Positions of the so-called "active region" for six Doppler scans discussed are shown. The S-band CP-2 radar is used for reflectivity data. Rawinsonde launch sites are shown at Grover (GRO) and Sterling (STK), Colorado, and Potter (POT), Nebraska.

July scans were begun at five-minute intervals, and each required about four minutes. The discussion here is restricted to six selected volume scans: three consecutive volume scans between 1623 and 1641 MDT, and three between 1704 and 1719 MDT. Data from CP-4 are not complete and are not used in this analysis.

Using software of Kohn *et al.* (1978), we interpolated measurements obtained in each volume scan to a common grid, shifted slightly to account for storm motion during the scan times, and then combined the data from the three radars to determine horizontal (u, v) components of air velocity. The vertical air velocity w was estimated by assuming $w = 0$ near the top of the data region and applying the mass continuity equation in a downward integration. The main emphasis here is on the structure in the middle parts of the cloud, so the volume scans have been assigned times appropriate for the mid-level w fields, which rely on data from the upper part of the scanned volume.

Errors in the air velocity components have been discussed in detail by Frank and Foote (1982), and are summarized here. The errors are thought to have rms values (over the entire data set discussed) of 2 to 3 m s^{-1} for u and v and about 5 m s^{-1} for w. Some sources of error are highly dependent on position, and maximum errors in w could be in excess of 10 m s^{-1}. A comparison of updraft measurements obtained from the Doppler radars and from the penetrating T-28 aircraft is presented in the next section, and further comparisons are given by Frank and Foote (1982). The measurements are in reasonable agreement, lending support to the major velocity features evident in the Doppler data, though for reasons discussed by Frank and Foote the comparison is not entirely straightforward.

Spatial resolution of the field of motion should be adequate to represent three-dimensional features (e.g., updrafts) larger than 6 km in diameter at better than 90% of their original amplitude. Features of smaller scale are attenuated more; for example, features less than 2 km across are damped by more than 50%. Distortion of the shorter-lived and generally smaller features of the velocity field is also likely as a result of the 4-min period needed to scan the whole storm.

Doppler measurements were made in most of the radar echo volume of the Westplains storm, but much of the discussion focuses on a cubical region, 15 km on a side, located in the forward (south) part of the storm. We refer to this as the "active region," since it contained the intense updrafts and downdrafts. The positions of the active region over the ground for each of the six volume scans are also shown in Fig. 1.

In this paper all velocities are displayed relative to the storm, which moves from 330° at 8 m s^{-1}. Where sequences are shown, the display area has been moved along with the storm.

3. The basic airflow pattern

In Part I of this study it was observed that certain basic features of the storm's reflectivity structure remained essentially unchanged for long periods relative to the apparent lifetimes of individual cells. We now address the similarly persistent aspects of the

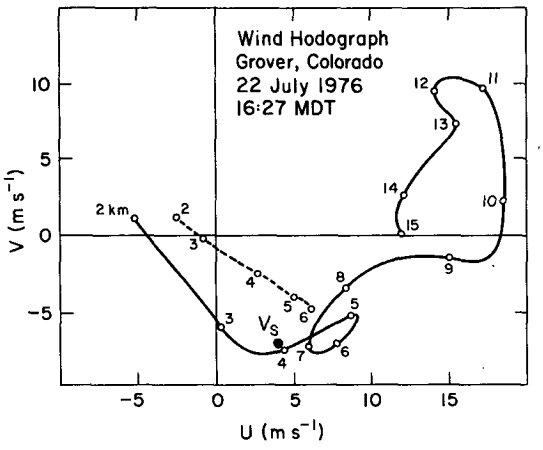

FIG. 2. Hodograph of environmental winds from the GRO sounding at 1627 MDT (solid line), heights given in kilometers (MSL). The dashed line shows data from the 1605 STK sounding, which is more representative at low heights. Mean storm motion is represented by V_S.

three-dimensional airflow deduced from the Doppler measurements.

Consider first the hodograph of the environmental wind in Fig. 2, taken from the 1627 Grover sounding; V_s is the storm motion in the period discussed here (approximately 1625–1720). In a coordinate system attached to the moving storm there is considerable veering with height in the lower levels (where the 1605 Sterling sounding, dashed, is most representative). The relative wind is south-southeasterly at about 10 m s^{-1} near the surface, westerly at less than 5 m s^{-1} in the middle troposphere, and southwesterly at 10–15 m s^{-1} in the upper troposphere.

To illustrate the basic storm airflow pattern we examine results from the 1635 Doppler volume scan. Fig. 3 shows a streamline analysis from Doppler data at 3.5 km MSL for the Westplains storm. The shaded region signifies updraft, as determined by Queen Air N306D flying just below the cloud base (see Wade and Foote, 1982). Most of the moist air entering the storm is thought to pass through this region, but there is no echo there at 3.5 km, and thus no Doppler data. The south-southeasterly relative motion in the inflow sector as measured by the Queen Air is shown schematically by the bold arrow. The southeasterly relative flow seen in Fig. 3 tends to be dominated by the motion of the storm itself toward that direction.

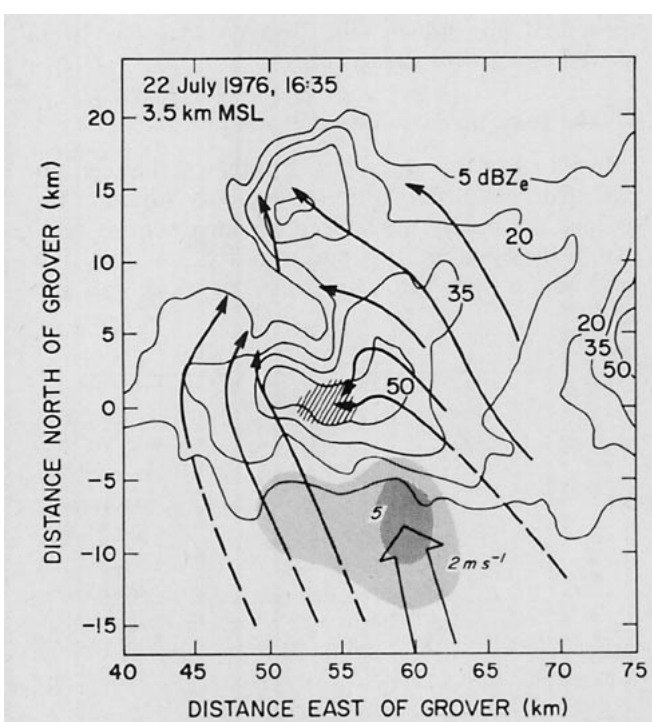

FIG. 3. Storm-relative airflow and reflectivity structure at 1635 MDT at 3.5 km MSL, near cloud base. Streamlines (dashed where data are not present) and downdraft (hatched for $w < -5$ m s^{-1}) are from Doppler observations. The area of updraft near cloud base (stippled) is mapped from aircraft data obtained during several traverses near this time. Bold arrow on the south represents the southeasterly inflow below cloud base. The streamlines do not generally represent trajectories, nor are they meant to depict the speed of the flow.

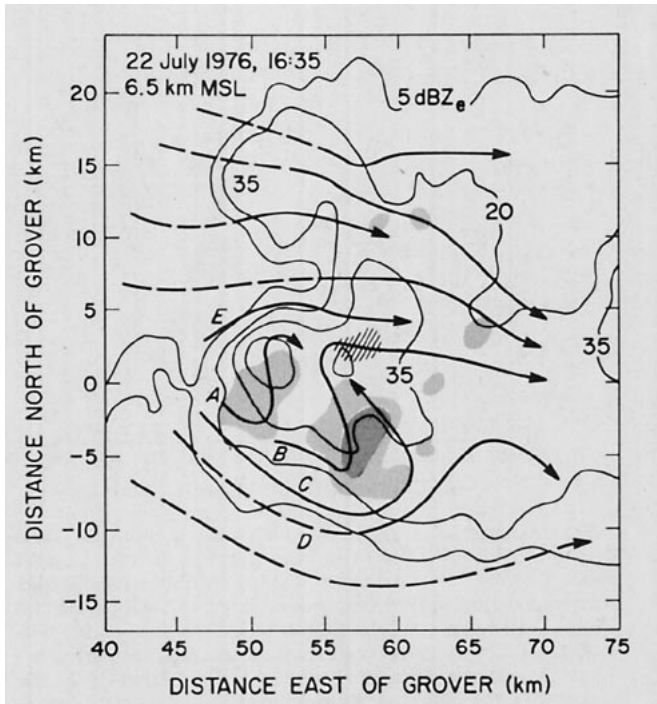

FIG. 4. Storm-relative airflow as in Fig. 3, but at 6.5 km. Updrafts shown for this altitude, which is near the height of maximum updraft, are from Doppler data. The streamlines designated by letters are referenced in the text.

An area of downdraft (hatched for $w < -5$ m s^{-1}) is situated in the region of highest reflectivity at this height, overlying an area of fairly strong horizontal divergence at the surface, nearly 5×10^{-3} s^{-1}. Confluent streamlines in the vicinity of the downdraft reflect convergence of air into it at this height, as will be discussed later. Part of the echo from the neighboring Storm II is seen on the right side of Fig. 3.

The updraft shown at cloud base is actually feeding two cells at the time of these data, as seen more clearly in Fig. 4 for 6.5 km altitude. Here the updraft has been determined from Doppler measurements. The two large areas of updraft, corresponding to Cells I and H as discussed in Part I, are directly linked to the updraft at cloud base. The eastern updraft (Cell I) is much the stronger of the two at this time, with a maximum speed of 29 m s^{-1}. According to reflectivity analyses the western Cell H has already passed its maximum intensity. Several other small updraft cores shown in the figure are not persistent, but the larger-scale pattern is similar from one volume scan to the next.

The streamlines of the horizontal flow at 6.5 km show large perturbations in the vicinity of the updrafts, with two features most evident: (1) the tendency for air coming from the west to pass around the updrafts, as in streaming flow past a barrier, and

(2) the southerly to southeasterly momentum apparent in the regions of updraft. These features have been previously reported in both field observations and numerical modeling results (e.g., Fankhauser, 1971; Kropfli and Miller, 1976; Moncrieff and Miller, 1976; Heymsfield, 1978; Brandes, 1978; Schlesinger, 1978, 1980; Wilhelmson and Klemp, 1981; Klemp *et al.*, 1981). The latter seems to reflect conservation of horizontal momentum as boundary layer air is lifted into the storm.

When viewing streamlines A, B, and C, which pass around the south side of the storm and then turn into the updraft, it should be remembered that they are distinct from air trajectories because of the strong component of vertical motion. The S-shaped streamlines like A and B in Fig. 4 seem to be characteristic of large storms that occur in an environment for which the wind profile relative to the storm veers with height. Similar patterns can be seen in the data of Eagleman and Lin (1977), Brandes (1978), Heymsfield (1978) and Lemon and Doswell (1979). In a veering environment such a pattern should be expected when the storm updraft is large enough that inflow momentum tends to be conserved in the updraft, and the environmental winds aloft are strong enough to produce the blocking effect, thereby leading to the cyclonic curvature of this streamline on one side of the storm and anticyclonic curvature on the other. Rotunno (1981) has recently considered certain aspects of this configuration from a theoretical viewpoint.

The region of general confluence downwind of the major updrafts contains a weak anticyclonic eddy. Such an eddy in the lee of an updraft has been previously reported by Lemon (1976a). In the present case this feature has a vertical extent of 1–2 km.

The horizontal section in Fig. 4, at an altitude of 6.5 km, is only 1 km below the level of maximum updraft, where horizontal divergence in the updraft is small. In contrast, Fig. 5 shows the streamlines at 9.5 km, about 2 km above the updraft maximum and 4 to 6 km below the storm top. The strongly divergent airflow in Fig. 5 illustrates the basic structure in the upper part of the storm. The streamline pattern is dominated by a source region on the south side of the storm, reflecting outflow from the major updraft. This source, superimposed on the southwesterly environmental flow at this altitude, produces a barrier-like flow pattern similar to that seen at 6.5 km. The anvil region is seen as an area of relatively weak reflectivity extending downwind from the updraft and reflectivity core.

The details of the Doppler wind field are shown in Fig. 6 for the active region. In the vertical motion field (center panels) the pattern is dominated by a single large updraft of dimensions 5 to 10 km across, extending throughout the depth of the storm. A weak-echo region, which is most obvious at the 6.5 and 8.0

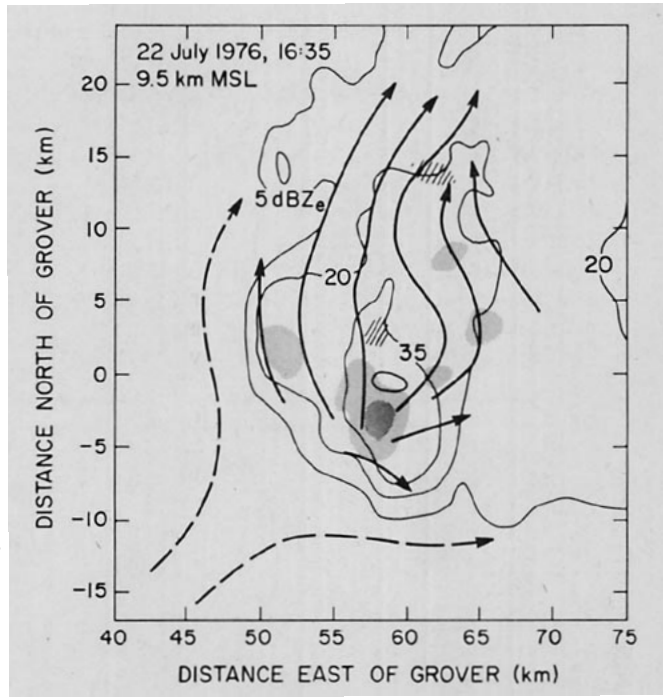

FIG. 5. Storm-relative airflow as in previous two figures, except here the height is 9.5 km, near the height of maximum upper-level outflow.

km levels, is centered on the updraft maximum, as originally proposed by Browning and Ludlam (1962). As discussed in Part I, though, the vault is never strongly developed in this storm and is not a persistent feature.

Two general regions of downdraft are observed in the middle levels, one to the north of the strong updraft and one just to the east. The northern downdraft is behind the sloping updraft (opposite the inflow side) in a region of high reflectivity where precipitation loading may be a contributing factor. The eastern downdraft is imbedded in the cyclonically streaming flow that has passed around the south side of the storm, and it occurs on the lee side of the updraft with respect to the environmental wind at mid-cloud level. It is probably influenced by evaporative chilling of the dry mid-level air during its traverse in a region of weak reflectivity around the south side of the storm, though other factors may also be important.

Downdrafts occurring within this cyclonically streaming flow have been reported for Oklahoma storms (e.g., Brandes, 1978; Heymsfield, 1978). In the Oklahoma studies downdrafts are observed farther upstream than in the present storm, i.e., to the south of the updraft along streamline C in Fig. 4, rather than to the east. This position is distinct yet from that of the so-called "rear-flank" downdraft inferred in some studies of Oklahoma storms (e.g., Barnes, 1978; Lemon and Doswell, 1979) to exist near the upwind stagnation point in the middle levels of the cloud (this

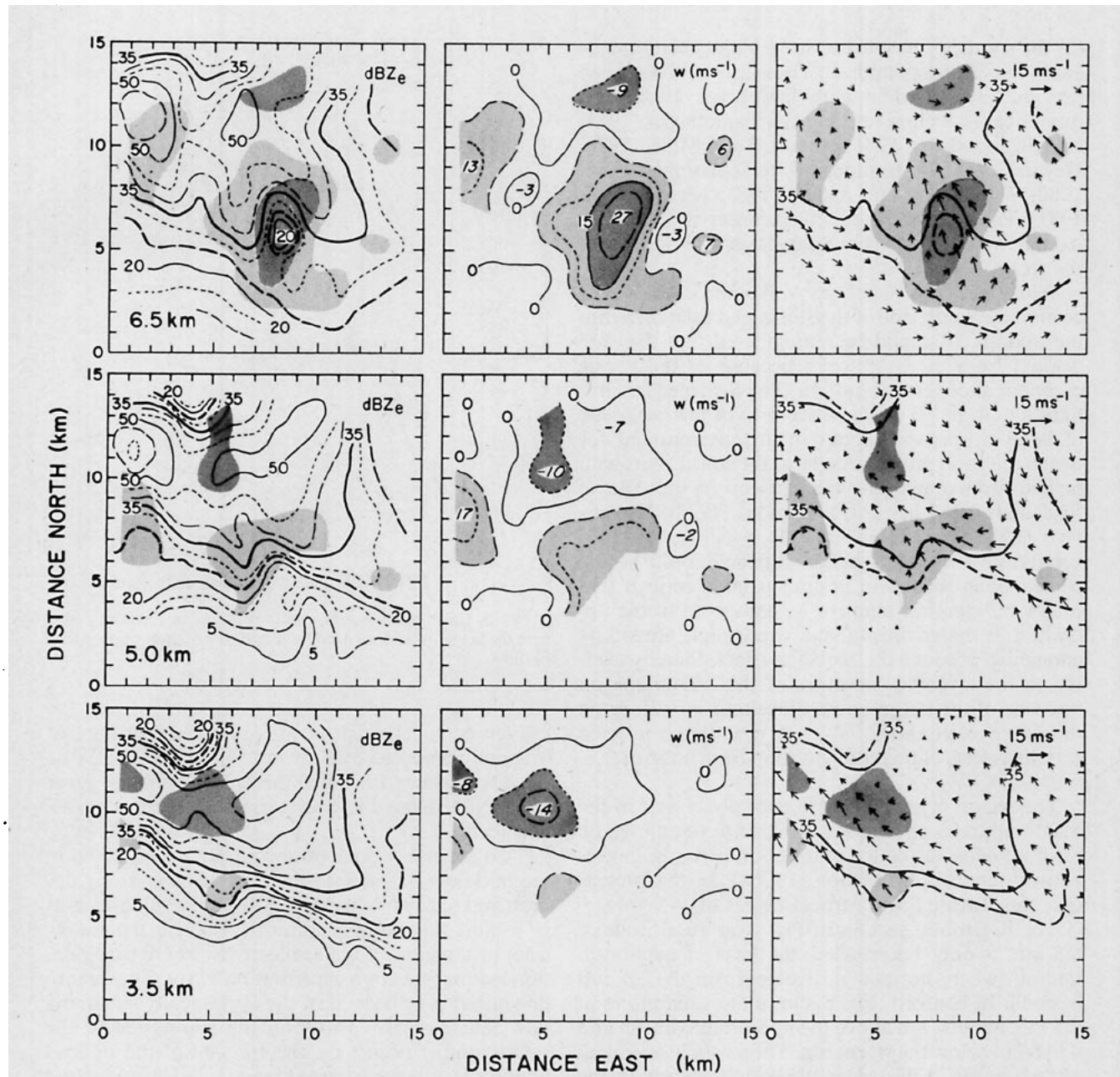

FIG. 6. Horizontal sections showing detailed storm-relative airflow and reflectivity in the active region at 1635 MDT, using data for six altitudes. The origin of the coordinate system is at (49 km, −10 km) relative to the Grover field site. Left: Radar reflectivity factor Z, contoured at 5 dB(Z) intervals. Center: Doppler-derived vertical air velocity w, contoured at 5 m s^{-1} intervals; extremes are labeled in italics. Right: Horizontal wind vectors; vector scale at upper right. Selected contours at Z and w are superimposed on other data for reference.

would more accurately be called the right flank for any storms that move significantly to the right of the winds, as in the present case).

Although Fig. 6 indicates that the eastern downdraft is weaker than the northern downdraft, at other times it is of the same magnitude or even slightly stronger. Observations from T-28 aircraft near the time shown indicate that it was in fact stronger than estimated from the Doppler data. Fig. 7 compares vertical air motion from the T-28 data with Doppler data collected during the 1640 scan sequence. Although the updraft magnitudes seem to be comparable, data from the T-28 lead to estimates as large as 14 m s^{-1} for the eastern downdraft, while the Doppler estimate is only about 4 m s^{-1}. Further comparisons of vertical motion from the T-28 and Doppler systems are given by Frank and Foote (1982).

At the lower levels, below about 5 km, the eastern

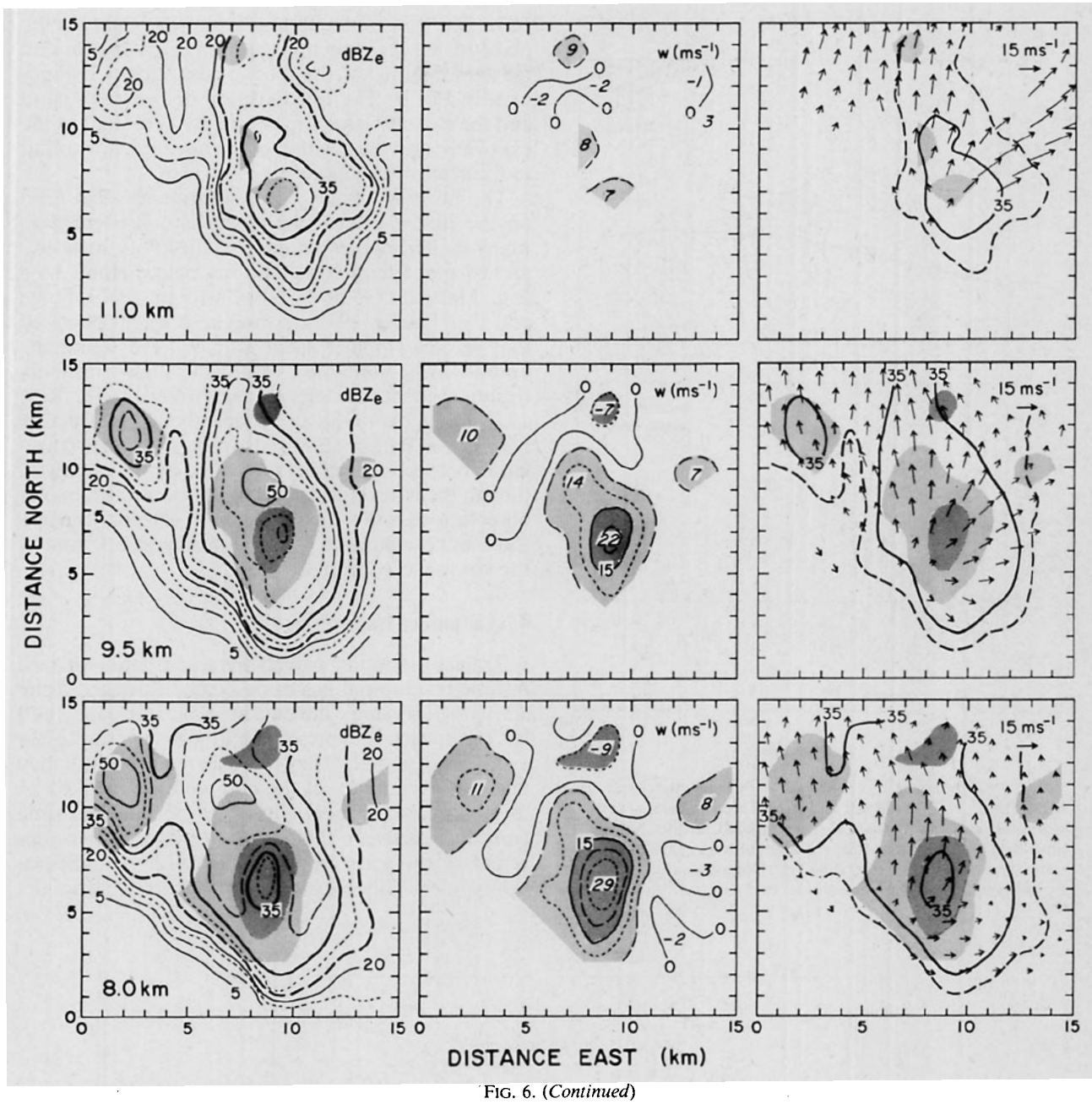

FIG. 6. (*Continued*)

and northern downdrafts tend to merge into a single region of downdraft elongated in a northwest–southeast direction. This is more obvious in the 1626 and 1640 data, shown in Fig. 8, than in the data for 1635. Air converges into this region from both the north and south sides of the storm, as evident in the 5-km winds in Fig. 6, to feed the surface outflow pool. This is shown more clearly by trajectory analyses in the following section.

An obvious feature of the downdrafts in Fig. 6 is their small size and strength relative to the main updraft. This has been observed in other Doppler studies of storms (for example, Miller, 1975; Kropfli and Miller, 1976), but downdrafts of intensity equal to that of updrafts have also been reported (Brandes, 1978). One reason for the weakness of the northern downdraft may be that it is poorly ventilated by the weak environmental winds relative to the storm, as seen in Fig. 4, so that evaporative cooling is perhaps not a strong contributing factor. While the eastern downdraft is apparently well ventilated, precipitation drag may be relatively unimportant there.

Fig. 9 shows a north–south cross section through both the main updraft and northern downdraft at

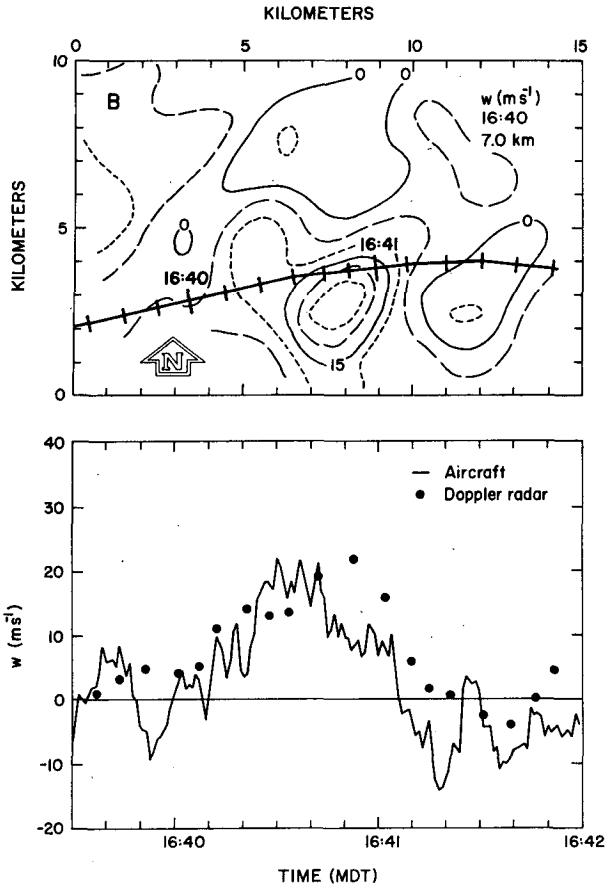

FIG. 7. Comparison of vertical air velocity estimates near 1640 MDT from the T-28 aircraft and triple-Doppler radars. Top: The storm-relative aircraft track is superimposed on the Doppler updraft field at 7 km MSL, near the flight altitude. Bottom: Aircraft estimates are represented by solid line; Doppler estimates obtained by bi-linear interpolation are shown as dots.

1635. The flow in the updraft is approximately in the plane of the cross section, as seen from Fig. 6, and the zero contour of the cross-plane velocity component in Fig. 9. The juxtaposition of the weak vault and the updraft is seen more clearly here than in the plan view, and the position of the northern downdraft to the rear of the updraft is also clear.

The position of the strong updraft in weak echo on the inflow side of the storm is consistent with many earlier studies based on reflectivity measurements and aircraft observations below cloud base (e.g., Marwitz, 1972a, 1972b; Chisholm, 1973; Foote and Fankhauser, 1973). However, it might be noted that several Doppler radar studies have found the updraft to be contained within the high-reflectivity region even at low elevations (Miller, 1975; Ray, 1976; Brandes, 1978), so apparently either structure is possible. Battan (1980) also notes no high correlation between reflectivity factor and updraft strength, though the latter study of vertically-pointing Doppler observations is in a slightly different category because there is no assurance that the strongest updrafts of the storm were sampled.

4. Air parcel trajectories

Trajectories of air parcels were calculated forward in time from initial positions located throughout the active region using wind data at 1626, 1635, and 1640 for 7 min each to represent approximately the 1622–1643 time period. They were extended until they reached a boundary of the data volume or until 21 min had passed. There appears to be sufficient time continuity between the successive wind data to represent storm-scale aspects of the airflow configuration, and we choose to consider these trajectories be-

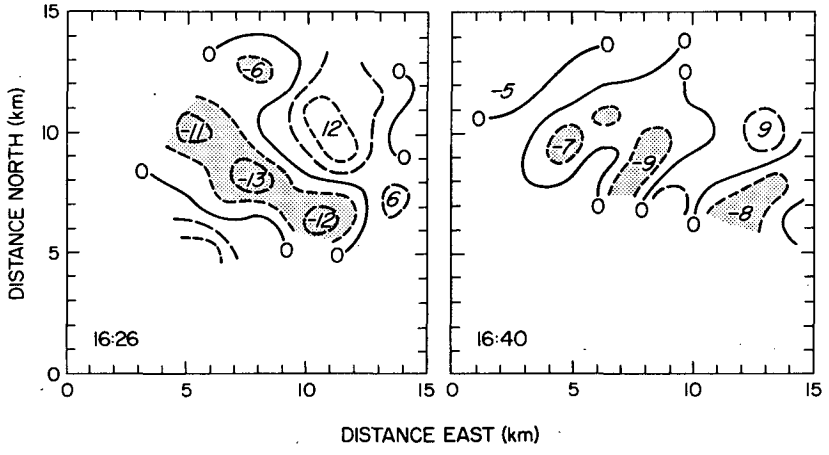

FIG. 8. Vertical motion field in horizontal sections at 3.5 km MSL for 1626 and 1640 MDT. The downdraft at this altitude represents a general merger of two distinct downdrafts noted at higher elevations. Contours are shown at intervals of 5 m s^{-1}, with downdrafts stronger than 5 m s^{-1} stippled.

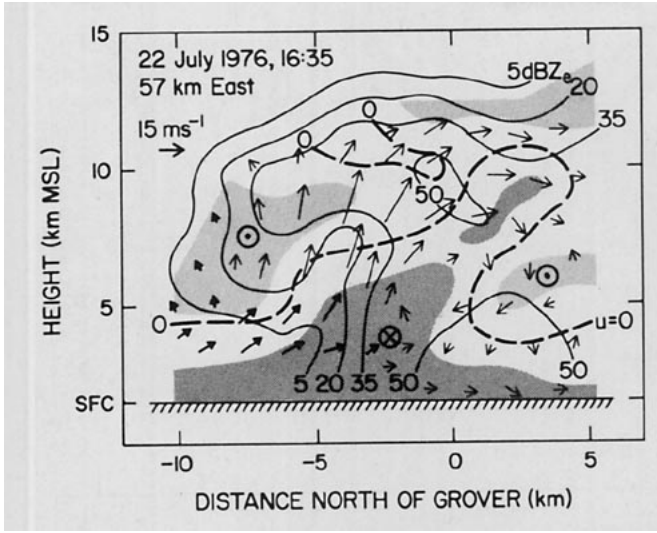

FIG. 9. Vertical section oriented south to north along $x = 57$ km showing the relative locations of the weak-echo vault, updraft, downdraft, and echo core. Reflectivity is contoured (thin lines) at 15 dB(Z) increments. The scale for the storm-relative wind vectors is shown in the upper left. Bold wind vectors with triangular arrowheads identify subjectively extrapolated velocity data. Dark stippling denotes horizontal flow greater than 5 m s^{-1} into the page, and light stippling denotes similar flow out of the page. The thick dashed line is the zero contour of flow normal to page.

fore discussing in the following section the question of temporal evolution. Doppler measurements were lacking below about 6 km in much of the updraft region on the south side of the storm, where reflectivity was relatively weak. Because this region is very important in understanding inflow trajectories, we interpolated and extrapolated the velocity data there by eye to fill data voids as shown, for example, by the bold vectors in Fig. 9.

Fig. 10 shows selected air parcel trajectories that illustrate the airflow pattern in the vicinity of the strong updraft of Cell I. Trajectories reaching the upper part of the storm are shown on the left, those confined mainly to middle heights are shown in the center, and downdraft trajectories are on the right.

Trajectories H1 and H2 are representative of air parcels that experience the strongest updraft. In 5 min they ascend from the cloud base to nearly 10 km, with a mean ascent rate of about 20 m s^{-1}. While passing through the updraft core they turn gradually to the right, and, upon reaching the upper levels of the storm, they exit toward the northeast (H2 must make a leftward turn in the upper levels after leaving the data region). Parcels following H3 and H4 ascend in the "shoulder" of the strong updraft, and their trajectories are more tilted away from the vertical. They reach positions above the mid-level reflectivity core about 10 min after passing through the cloud base and then level out to leave the active region toward the north at an altitude of about 10 km. Parcels following H5 and H6 ascend on the west side of the updraft core at about the same rate as H3 and H4, but their trajectories show little tilt until they reach the upper levels. Above ~8 km trajectories H5 and H6 diverge toward the north and south, respectively, as they approach the divergent upper part of the main updraft core from the west side.

On the whole, air parcels comprising the updraft branch of the flow follow a rather simple path in the storm-relative framework. They approach from the south-southeast and retain southerly momentum as they rise, such that the updraft tilts toward the back of the storm. They veer gradually (by 30° to 90°) as they ascend and exit the storm toward the north and northeast. Trajectories in the south and southwest parts of the updraft are more erect, and tilt toward the east under the influence of westerly flow around the south perimeter. While they represent a rather small proportion of the updraft flux they nevertheless may be important in terms of particle transport and microphysical structure.

It might be noted that the simple veering with height of the principal updraft trajectory, H1, occurs despite the fact that the updraft possesses predominantly cyclonic vorticity of magnitude typically (4–10) × 10^{-3} s^{-1} in the middle levels of the storm. Klemp *et al.* (1981) have illustrated the same phenomenon in cloud model and multiple-Doppler results. Similar updraft trajectories have been proposed by Marwitz (1972a) and Browning and Foote (1976), in contrast to the cyclonically rotating (strongly backing) trajectories inferred by Browning (1964). However, trajectories similar in sense of rotation to those of Browning (1964) have since been reported in the multiple-Doppler analysis of Brandes (1981), so apparently both types can occur. Heymsfield (1978) also infers a cyclonically turning updraft trajectory, but as shown here the existence of positive vorticity in the updraft is not sufficient to guarantee this. The storm model of Eagleman and Lin (1977) showing a cyclonically spiraling updraft is erroneously based on so-called "perturbation winds" and is not consistent with the basic data.

Parcels ascending in weak updrafts on the front and right front flanks are represented by trajectories M1 and M2, which enjoy rather long residence times in the middle heights as they follow cyclonically curved paths around the periphery of the updraft region. Special emphasis has been placed on trajectories like M1, which rises on the west and passes over the principal inflow region. As discussed by Browning and Foote (1976), particles attaining large enough terminal velocities along such a path could descend into the southeasterly inflow and be carried into the strong updraft where further growth into hail is possible. Trajectories like M1 and M2 probably often originate in young cumulus turrets on the flanks of the mature storm.

Trajectory M3 illustrates the nature of mid-level

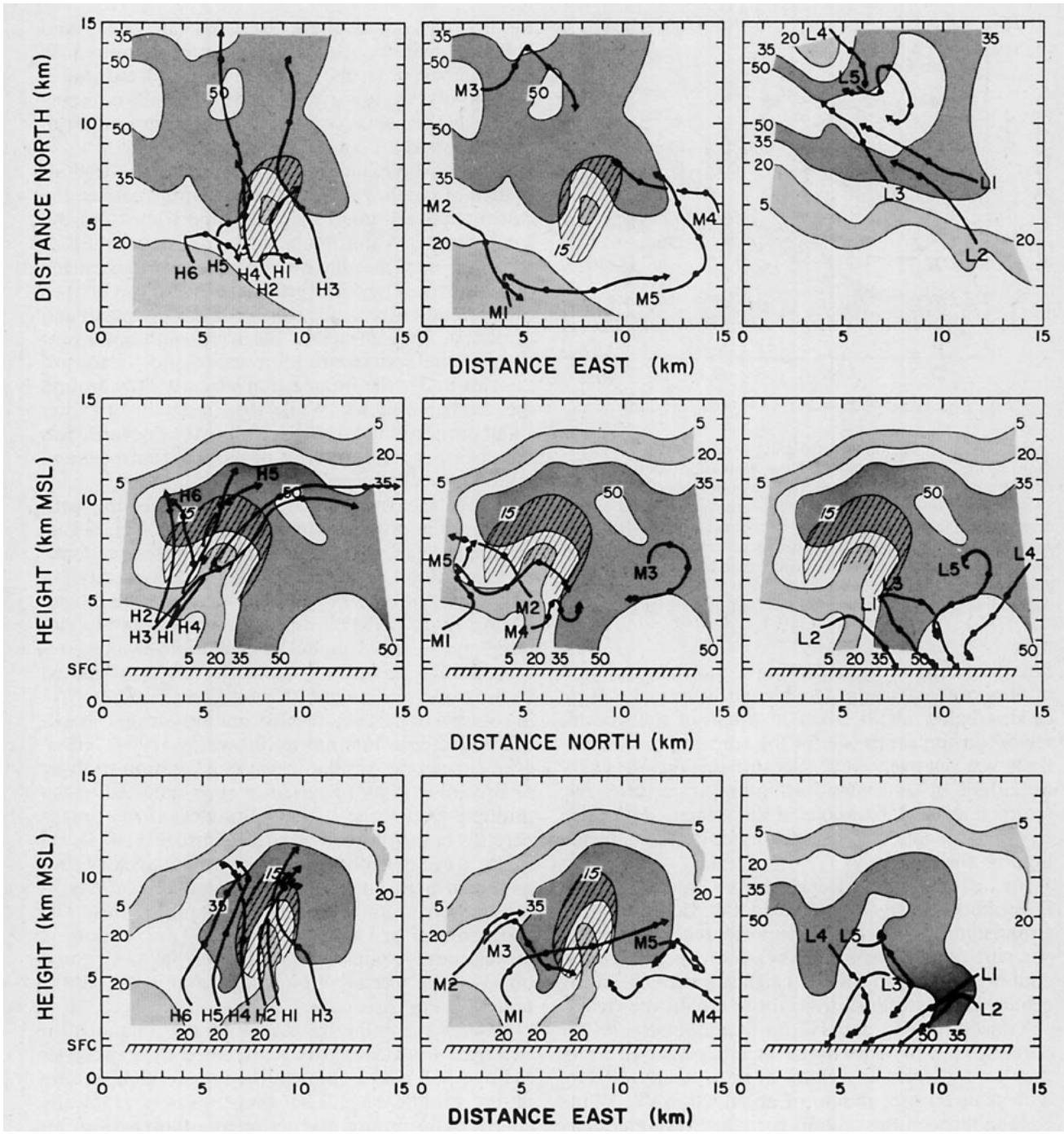

FIG. 10. Air parcel trajectories calculated from Doppler wind fields for 1626, 1635 and 1640 MDT. The top row shows the trajectories in plan view; the middle and bottom rows show projections on vertical planes oriented north-south and east-west as indicated. The left column depicts updraft trajectories that are initiated at 3.5 km MSL, about the altitude of cloud base. The middle column shows trajectories that reside mainly in middle levels. The right column illustrates the dominant downdraft trajectories. Dots along the trajectories indicate 5 min time intervals. Reflectivity contours and updraft location (hatched for $w > 15$ m s^{-1}) are from the 1635 scan sequence. They are shown for an altitude of 6.5 km MSL for the left and middle frames of the top row, and for 3.5 km on the right. In the center row the contours are for the plane passing through the updraft maximum, $x = 8$ km in the coordinates of this figure. In the bottom row the contours are for $y = 6$ km (left and center frames), and $y = 11$ (right frame).

flow around the north side of the updraft region. Originating in an area of weak updraft on the back side of Cell H, it follows a helical path as it subsequently descends and then approaches the main updraft from the back side. Other trajectories (not shown) in this region of the storm suggest that some

air parcels could undergo at least two successive up-and-down excursions along trajectories similar to M3.

Inflow to the storm at low to middle heights on the southeast side of the updraft is represented by trajectories M4 and M5. M4 begins at cloud base height in the relatively inactive region to the east of the updraft, and M5 traverses the eastern side of the updraft in the middle levels. Both of these arrive after about 20 min at positions on the east side of the downdraft region (see Fig. 8). It appears that parcels following trajectories like these might subsequently descend into the low-level outflow layer along trajectories like L1, which is initiated near the endpoints of M4 and M5. Trajectory L2 enters the radar echo at cloud base near the eastern edge of the updraft and L3 is initiated on the north edge, so that they rise slightly before entering the downdraft. Trajectories (not shown) originating around cloud base height in the region to the east and northeast of the updraft also descend to the surface.

It appears that the group of trajectories just discussed, including M4, M5, L1, L2, L3, and others originating at lower heights, account for a major proportion of the air that reaches the low-level outflow layer. It is not possible from this analysis to determine the exact origin in the storm's far environment of air contributing to this branch of the circulation, but these trajectories suggest that the low-level outflow is comprised of a mixture of air from middle levels down to the surface. Fig. 11 shows schematically some of the possible trajectories by which air can reach the low-level outflow area. By reference to the larger-scale flow shown in Fig. 4 and trajectory M5, it appears that some of this air originates in the mid-level environment (5–7 km) to the west of the storm, passes around the updraft approximately along streamline D in Fig. 4, and then descends in the leeward wake region (path B in Fig. 11). Along such a path it would presumably be mixed with cloudy air on the south and east sides of the updraft, and would be chilled by evaporation of cloud material as a result. Trajectories M4 and L2 seem to reflect a direct intrusion from the southeast of air originating near the cloud base height (path A). Trajectory L3 begins in the north shoulder of the updraft at cloud base where, according to the aircraft observations reported by Wade and Foote (1982), air is not convectively unstable. Subjective extrapolation of trajectory L3 backward suggests it may have originated in cold outflow spreading westward from Storm II. Surface data (Wade and Foote, 1982) indicate that this air might have been lifted over the outflow from the Westplains storm and into the back side of the updraft along path D in Fig. 11. Some air following trajectories like L2 could also have a similar history.

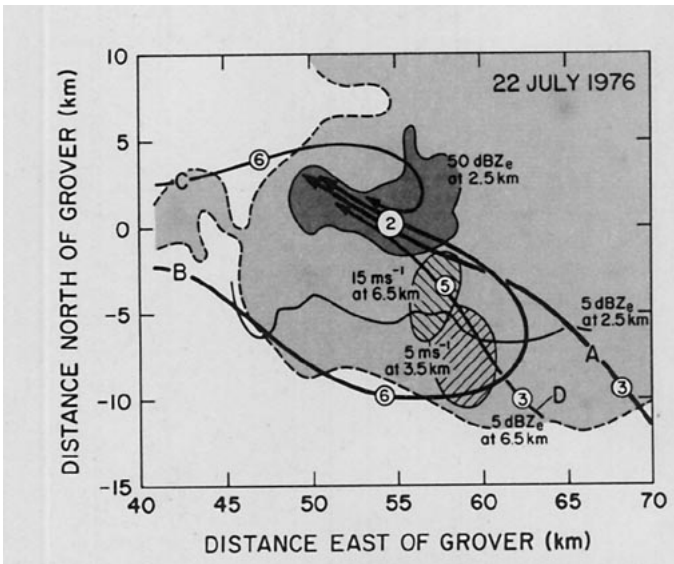

FIG. 11. Plan view indicating the principal downdraft trajectories. Paths A, B, C and D converge into the region of high reflectivity as they descend to near the surface. Circled numbers denote approximate heights in kilometers. The solid contours represent reflectivities of 5 and 50 dB(Z) at 2.5 km MSL. The dashed line is the 5 dB(Z) contour at 6.5 km. The updraft cores at 3.5 and at 6.5 km are shown as hatched regions.

Downdraft trajectories L4 and L5 indicate that some of the low-level outflow also comes from the northwest side of the storm along path C in Fig. 11, entering at heights below about 7 km (again, many trajectories reaching the outflow layer originate at lower levels than those shown). Extrapolating these trajectories backward, they appear to enter the storm system approximately following streamline E in Fig. 4, the anticyclonic branch of the barrier flow. Considering that the rate of descent along these trajectories is only about one-half that of the ones coming from the southeast, and that fewer trajectories in the northwest region are found to reach the surface layer, it seems that this branch provides a smaller contribution to the downdraft and outflow in the active region than does the branch on the southeast side of the storm. However, additional downdraft to the north of the active region, not considered here, would also probably ingest air from the northern (anticyclonic) branch of the mid-level barrier flow.

The convergence of paths B and C in the downdraft region is a reflection of the velocity field shown for the 5-km level in Fig. 6. One notes from Fig. 11 the interesting result that some of the mid-level streaming flow that is forced to part on the upwind side of the storm is apparently reunited in the vicinity of the reflectivity core, with both branches contributing to the low-level downdraft and surface outflow. The dominant southern branch of this pair is the same as the downdraft trajectory proposed in the schematic model of Browning (1964), being wrapped around the strong updraft. Analysis of multiple-Doppler radar observations of a storm in Oklahoma led Heymsfield (1978) to deduce two downdraft trajectories qualitatively similar to branches B and C in Fig. 11.

5. Evolution of the motion field in the active region

To examine the evolution we now consider two sets of triple-Doppler data, each including three consecutive volume scans. The first set, consisting of scans at 1626, 1635 and 1640, has been emphasized in previous sections because the data are more complete. It spans the time period corresponding to Cell I as discussed in Part I. The second set is comprised of scans at 1707, 1712, and 1718, and relates similarly to the K series of Part I.

a. The 1626–1640 period

We illustrate the evolution here with horizontal sections at 6.5 km (Fig. 12), and vertical cross sections through the strong updraft along the north–south (Fig. 13) and east–west (Fig. 14) directions. Reflectivity factor, Z_e, is shown on the left, vertical velocity w in the middle, and projected storm-relative wind vectors on the right. Selected contours of vertical velocity and reflectivity are repeated in other plots for reference. In the vertical sections, the shading rep-

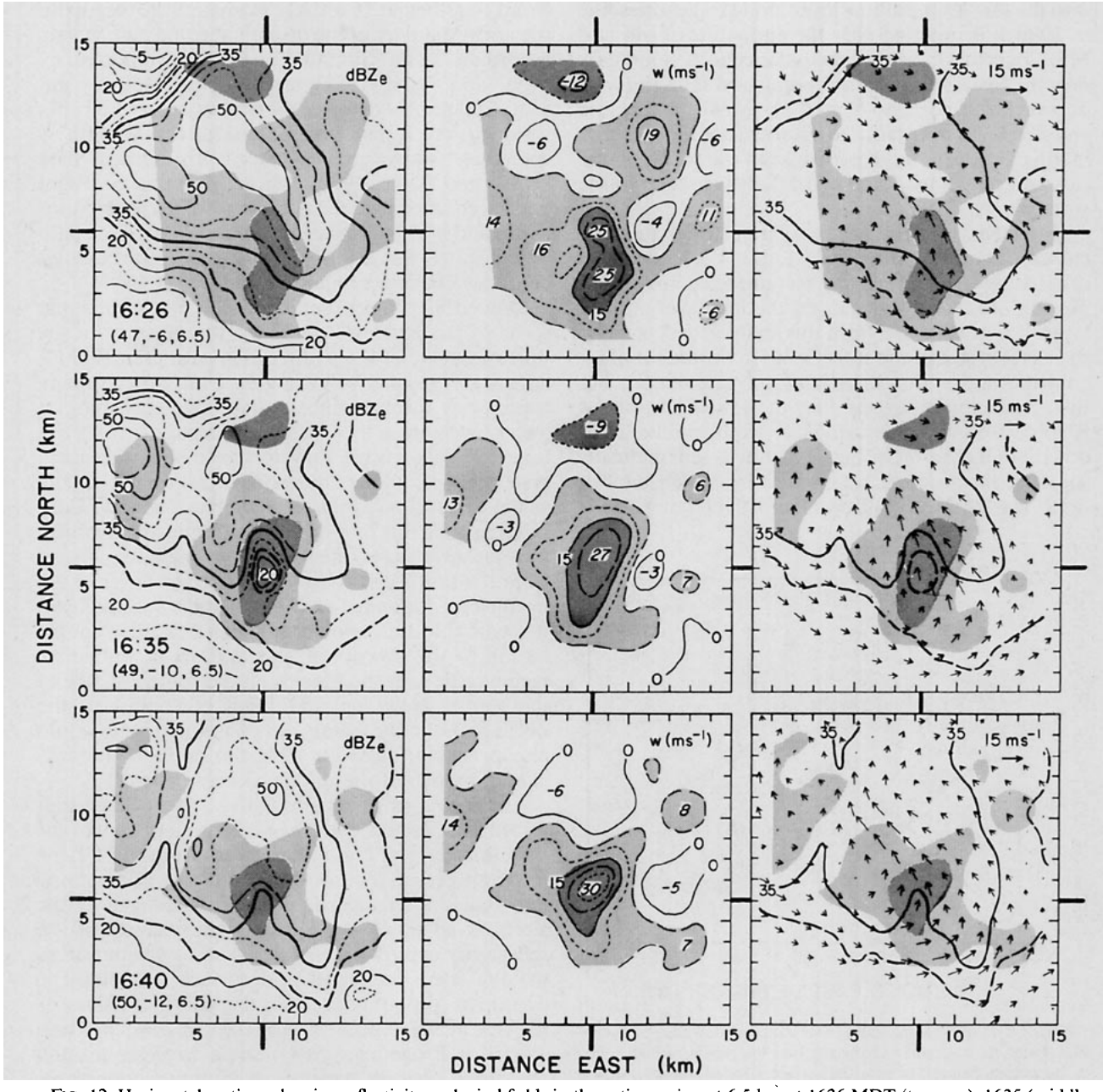

FIG. 12. Horizontal sections showing reflectivity and wind fields in the active region at 6.5 km at 1626 MDT (top row), 1635 (middle row), and 1640 (bottom row). The format is the same as in Fig. 6. The coordinates of the local origin with respect to Grover and elevation (MSL) are given in kilometers at the lower left of each row. Heavy tick marks on the perimeter of the grid indicate the locations of vertical sections shown in Figs. 13 and 14.

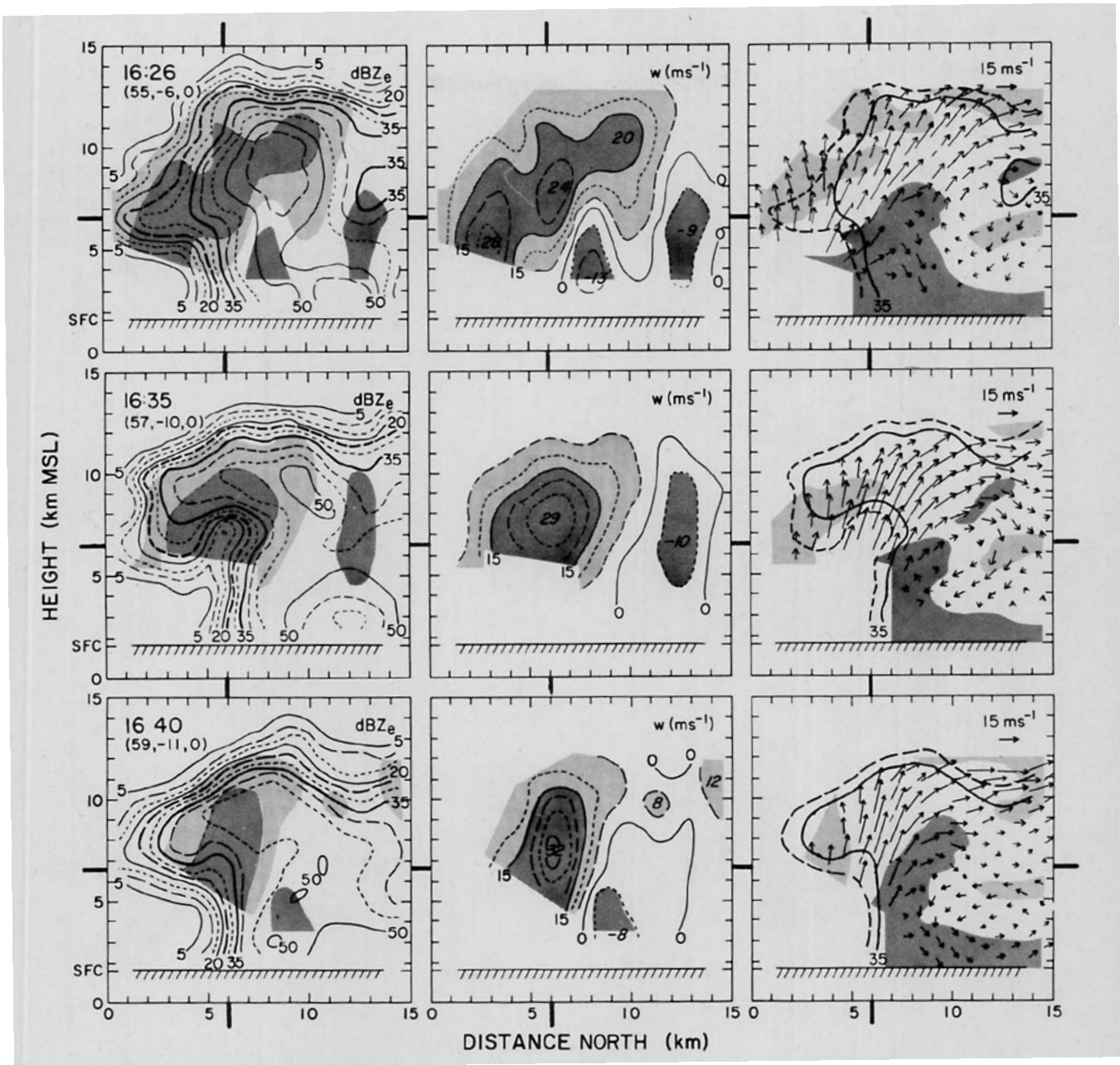

FIG. 13. Vertical sections south to north through the updraft core in a format similar to that of Fig. 12. The dark shading in the frames on the right indicates where the component of the flow into the page is greater than 5 m s^{-1}; light shading indicates flow out of the page of more than 5 m s^{-1}.

resents the cross-plane component of motion, rather than *w*.

We consider first the horizontal sections at 6.5 km in Fig. 12; the middle row for 1635 was discussed in Sec. 3. There are two major cells in the reflectivity plots, Cell H on the left, and the G–I sequence on the right, as discussed in detail in Part I. At 1626 updraft maxima are shown just south of the reflectivity cores for both of these cells. The updraft for Cell I is not as regular as at 1635, and a continuous band of updraft connects the two cells, in contrast with the discrete updrafts observed later at 1635. A fairly large updraft is also delineated on the northeast side of the echo core at 1626 (marked in the center figure with a 19 m s^{-1} maximum). It cannot be determined whether this is a remnant of some previous cell (perhaps part of Cell F), or merely a short-lived feature that did not persist long enough to produce a characteristic cellular echo. Only weak updrafts are seen in this position at other times.

The updraft structure at 1640 is little changed from that at 1635, with a single updraft core for Cell I

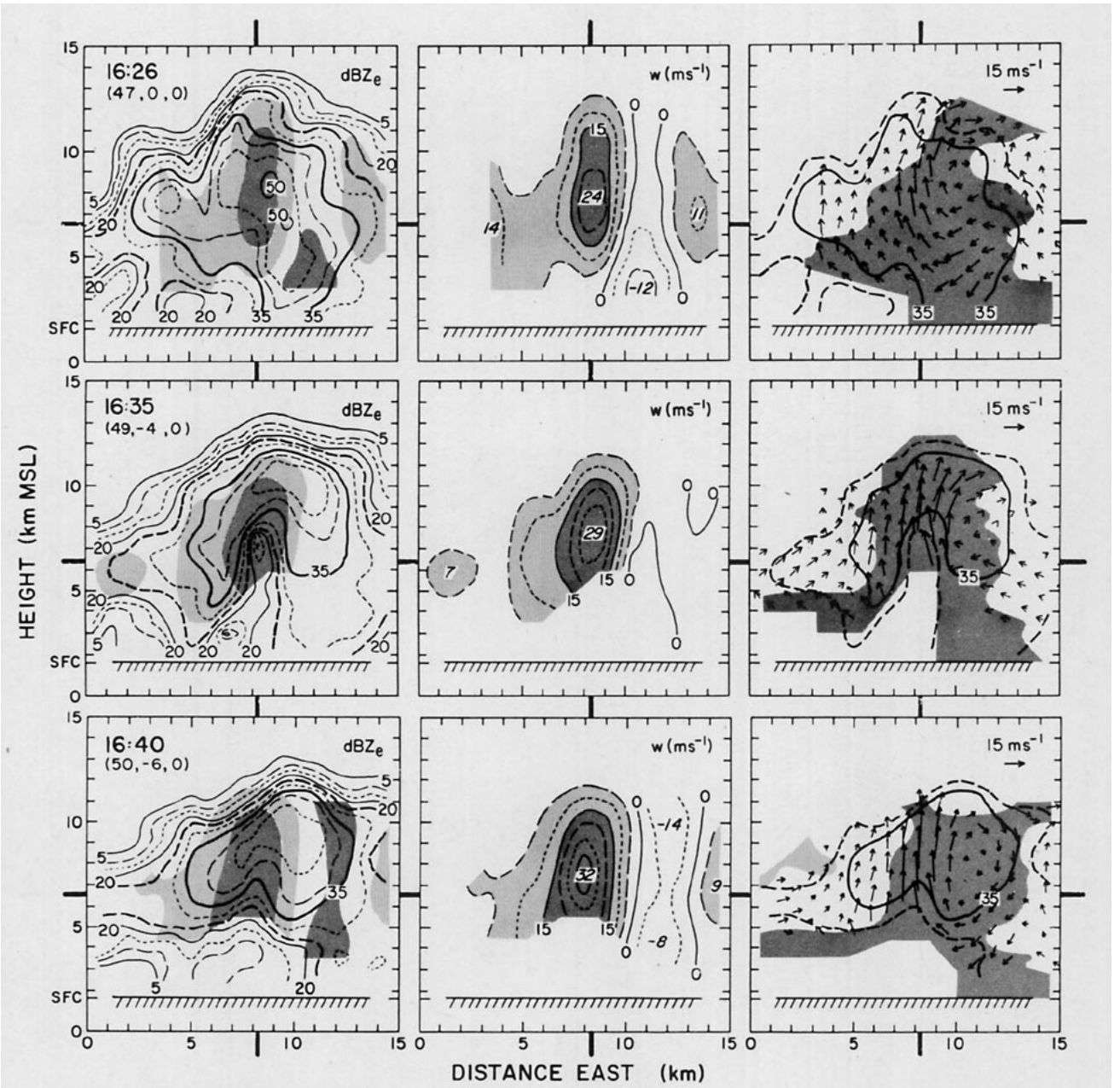

FIG. 14. Vertical sections west to east through the updraft core, similar to Fig. 13.

dominating the field in a position coincident with the weak-echo region, seen on the left. At all three times the dominant updraft is 5 to 10 km across, with a maximum speed of 25–30 m s^{-1}. Downdrafts are always present on the east and north sides of the strong updraft, as discussed previously.

The horizontal wind fields are all characterized by southeasterly (low-level inflow) momentum in the vicinity of the updrafts and cyclonic flow (westerly on the south sides turning to southerly on the east sides) around the major updrafts, as noted in the previous discussion for 1635, though the cyclonic turning of the flow is somewhat less pronounced at 1626.

The strong updraft appears with about the same size and intensity and in the same relative position in the storm at the three times, and the horizontal wind field shows only minor variations between the volume scans. Thus, it appears that the macroscale organization of the storm is basically steady in this period. Some deviations from the mean structure are observed in both the updraft and reflectivity structure, however, and more detailed consideration of these below will be useful.

The vertical structure of the storm in the vicinity of the updraft is shown in Figs. 13 and 14, in sections that pass through the updraft maximum. Since the

horizontal flow in the updraft is dominated by southerly momentum, Fig. 13 is the more revealing, as the wind vectors in the panel on the right are fairly representative of streamlines. The shaded areas on this panel represent flow of more than 5 m s^{-1} into or out of the plane, primarily below or above the updraft core. Fig. 14 aids the interpretation of the three-dimensional flow.

The most striking time-dependent features in the vertical sections are seen at 1626 and 1635. Changes of the updraft structure between these two times and the development of the vault in the region of the updraft core between 6 and 8 km altitude elucidate the nature of the cellular propagation discussed in Part I. On the basis of detailed reflectivity analyses there, it was concluded that the evolution of the updraft can be understood in terms of a steady upward flow with superimposed fluctuations. The fluctuations give rise to variations of radar reflectivity in the storm, and the steady component of the flow accounts for persistence of the basic mean structure. The Doppler updraft analyses support and clarify this picture, with the data for 1626, in particular, being the key. The 1626 view represents a time just before the reflectivity perturbations associated with Cell I are evident. Subsequent development of the reflectivity structure, discussed in Part I, is as follows. A small vault forms in the underside of the radar echo overhang, implying an updraft intensification starting in the lower levels, and then a local reflectivity maximum form over the vault. The height of the echo top and the visual cloud top both increase as this occurs. These observations seem to be consistent with the updraft evolution seen in Fig. 13 and interpreted further in Fig. 15 where intermediate and adjoining times are added subjectively.

In Fig. 15 four updraft impulses are labeled α through δ. Three of these relative maxima, α, β, and γ, are seen in the data at 1626. It appears that γ is the impulse that corresponds to Cell I in the reflectivity analysis, and that α and β have a correspondence with an earlier Cell G. The exact correspondence of G with α and β can not be determined from these data, but the appearance of γ with a maximum at a relatively low level seems to explain the weak-echo vault seen clearly at 1635. As the impulse γ rises it disturbs the trajectories of growing precipitation particles, pushing them upward locally and changing the reflectivity profiles accordingly. The vault starts developing about 1630, and the time history of γ as sketched in Fig. 15 seems about right for this. By 1630 α probably would have dissipated, to be replaced by β.

At 1635 γ is at maximum development, with perhaps a trace of β still evident in the Doppler data. The movement of α and β to the north in the figures can be attributed to the fairly strong component (10–15 m s^{-1}) of the relative environmental wind in this direction at the upper levels. At 1640 the size of γ seems to have diminished in its upper part, and by extrapolation of the updraft contour downward one can imagine a new impulse δ taking shape. In fact, the existence of δ is strongly supported by the aircraft measurements taken at cloud base and discussed by Wade and Foote (1982). At this time the updraft core at cloud base has moved further south from the precipitation as shown by the bold arrow for the 1640 plot in Fig. 15, and does not appear to support γ directly. Earlier aircraft analyses show the updraft closer to the echo at cloud base, for example as indicated by the bold arrow in the 1626 plot. Though no Doppler analyses are available for 1645 and 1650 we visualize the subsequent structure of δ to be similar to that hypothesized at 1630 and measured at 1635 for γ. The development of impulse δ would then be responsible for the vault associated with Cell J, first noted at about 1645 (see Part I).

b. The 1707–1718 period

The results from this time period are now examined to document the temporal changes that occur, and to ascertain the extent to which the storm-scale airflow deduced earlier persisted. During this period the vault associated with Cell K was already evident by the first volume scan, 1707, and it is not possible to verify whether the pattern of evolution just discussed was responsible for it. As discussed in Part I, the storm echo showed more small-scale structure during the 1707–1718 period corresponding to the intensification of Cell K than it did during the 1626–1640 period just considered. Since the increased structure in the reflectivity field was probably caused by the presence of additional smaller updrafts, we would expect the vertical motion field also to show more structure during the later period, and this is indeed the case.

Fig. 16 shows the Doppler data at 6.5 km altitude for the later period. The data on the southern side of the storm are generally less complete than in the earlier period, and additional plots are shown in Fig. 17 for 8.0 km, where more of the updraft is detected.

At 1707 the Doppler results show a broad region of updraft across the whole south to southwest side of the storm, containing two general updraft cores. The one on the southwest lies within an arm of reflectivity that is developing southward from the echo core. This is the echo feature associated with J_1 and K_2 in Part I. Fig. 17 shows that the updraft on the south side is deeper than that on the southwest and considerably stronger aloft. The southern updraft is in the same relative position as the large updraft in the earlier period (1626–1640), and is apparently responsible for the developing vault seen in its location at 1712. The existence of two updraft cores implies that some sort of discrete propagation has taken place,

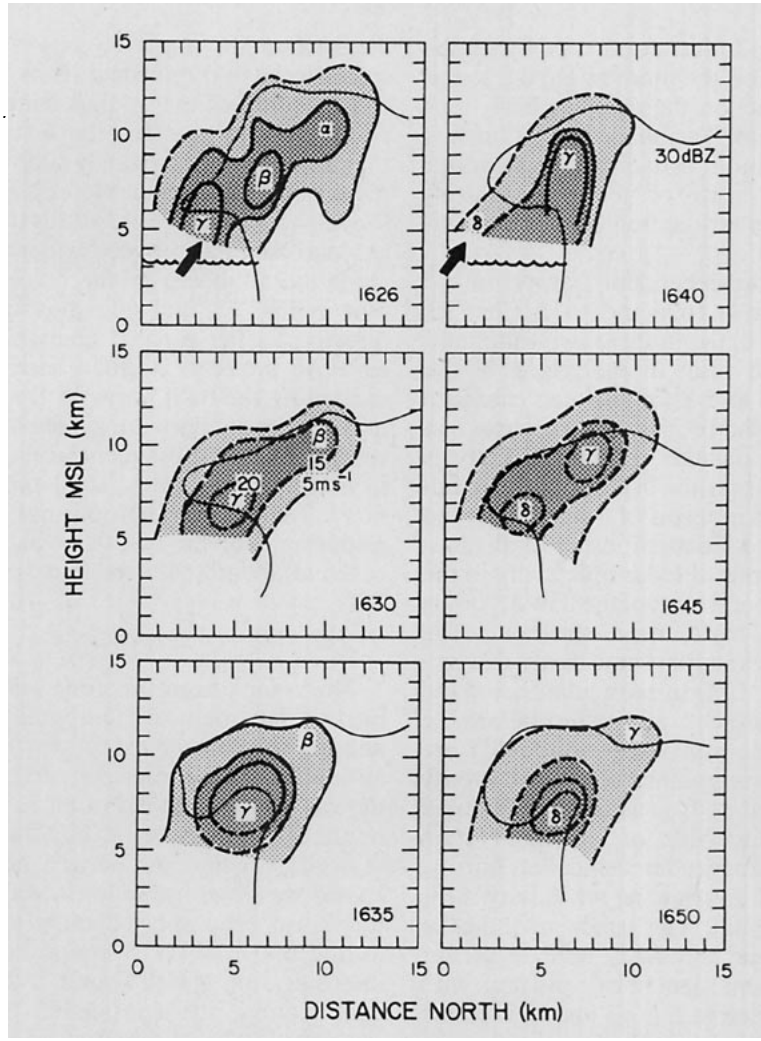

FIG. 15. Vertical sections (south-to-north) showing the proposed updraft evolution from 1626 to 1650 MDT. The thick solid lines (1626, 1635, 1640) are contours of vertical air velocity w based on the Doppler measurements of Fig. 13. Dashed lines are hypothetical contours of w. Thin lines are the measured 30 dB(Z) contour of reflectivity. Bold arrows at 1626 and 1640 show the position of the updraft core at cloud base as ascertained from aircraft measurements. Four updraft maxima are identified as α, β, γ and δ.

but the continuity in the radar echo and in the relative position of the southern updraft make it appear probable that this updraft evolved in a manner similar to that depicted in Fig. 15. The two maxima in the southern updraft at 6.5 km (the one on the left is only partially revealed) seem to correspond with reflectivity minima seen in the developing vault at 1707 and 1712. An arm of the southern updraft extends to the northeast at 1707, and at 1712 a discrete updraft is observed there.

At 1718 the vault has become filled with echo. The large updraft is now observed more on the southwest corner of the storm, and the updraft that was on the southwest at 1707 has lost its identity, perhaps merging with the larger updraft. A new updraft has appeared to the east of the large one, and a small weak-echo region is associated with it. This updraft gives rise to the echo of Cell K_4 mentioned in Part I. The existence and, in fact, the general strength of both updrafts is confirmed by the T-28 aircraft data collected between 1714 and 1716 (Heymsfield and Musil, 1982). Cell K_4 never becomes as large as Cell K, in fact within 10 min both K and K_4 are dissipating rapidly.

The cyclonic turning of horizontal winds near the updraft region in the 1626–1640 period is present also in the 1707–1718 period. In fact it is generally more pronounced in the later period, and the direction of flow on the north side of the updrafts is more easterly. In addition, westerly flow on the south sides is stron-

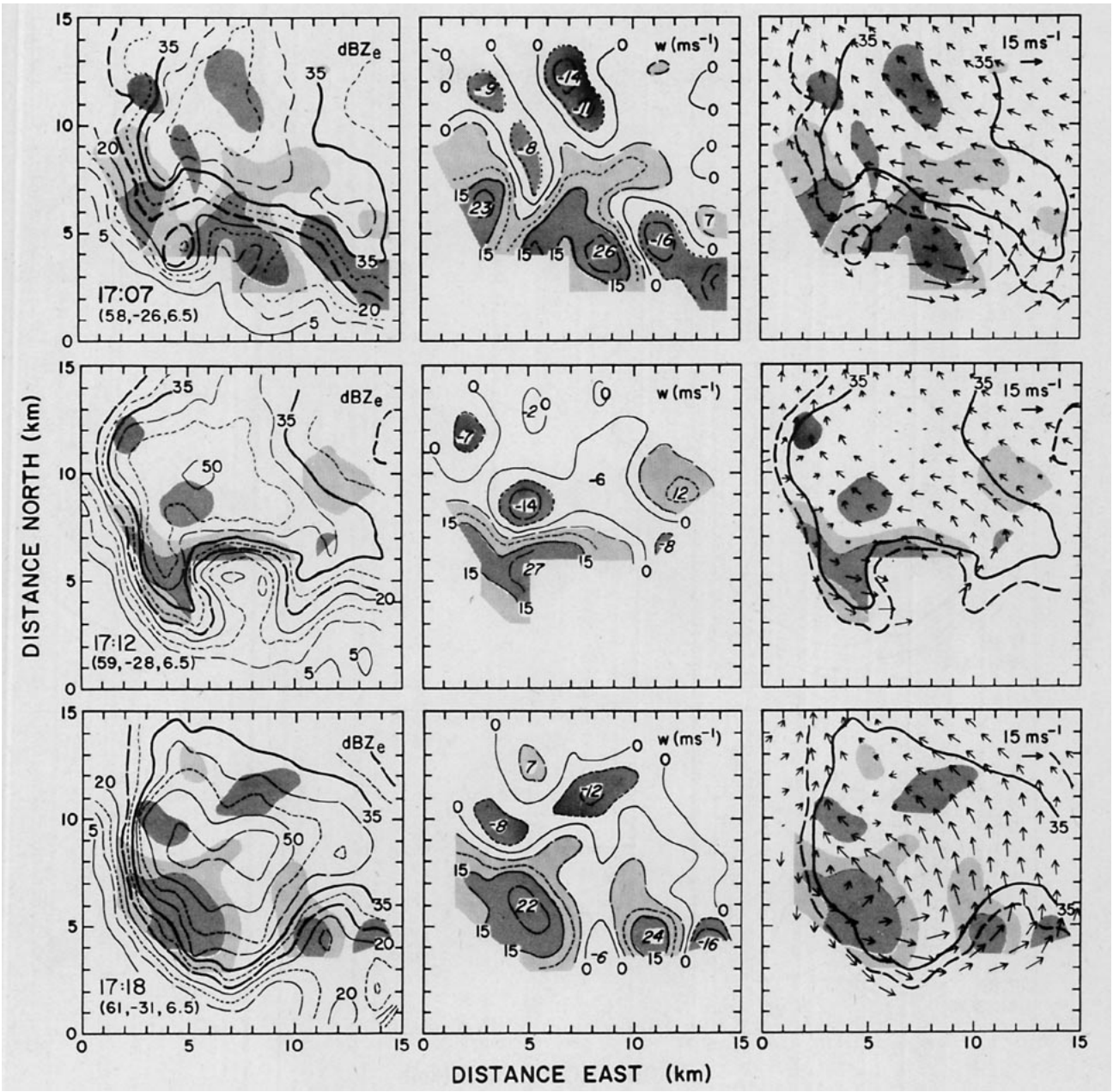

FIG. 16. Horizontal sections of the active region at 6.5 km MSL at 1707 MDT (top row), 1712 (middle row) and 1718 (bottom row) as in Fig. 12.

ger and penetrates well into the strong updrafts. These westerly speeds are about four times greater than those in the environment at this altitude, as judged from the hodograph in Fig. 2, and they can not be explained solely in terms of the barrier effect unless the environmental wind has increased substantially. Downdrafts are also more intense in this period, especially to the east of the updraft region.

Thus, though there are a number of specific changes one can point to in the details of the motion field between the two time periods, the basic airflow patterns, including a large, persistent updraft, are similar. Though the large updraft dominates the field of vertical motion, it is not isolated, but tends to be accompanied by somewhat smaller peripheral updrafts (for example, those associated with the dissipating Cell H during the 1626–1640 period, and with Cells K_2 and K_4 during the 1707–1718 period; see Part I for more details on these cells). It is highly probable that many other small, short-lived updrafts exist that cannot be resolved using the present data (Battan, 1980). In terms of hail, these peripheral up-

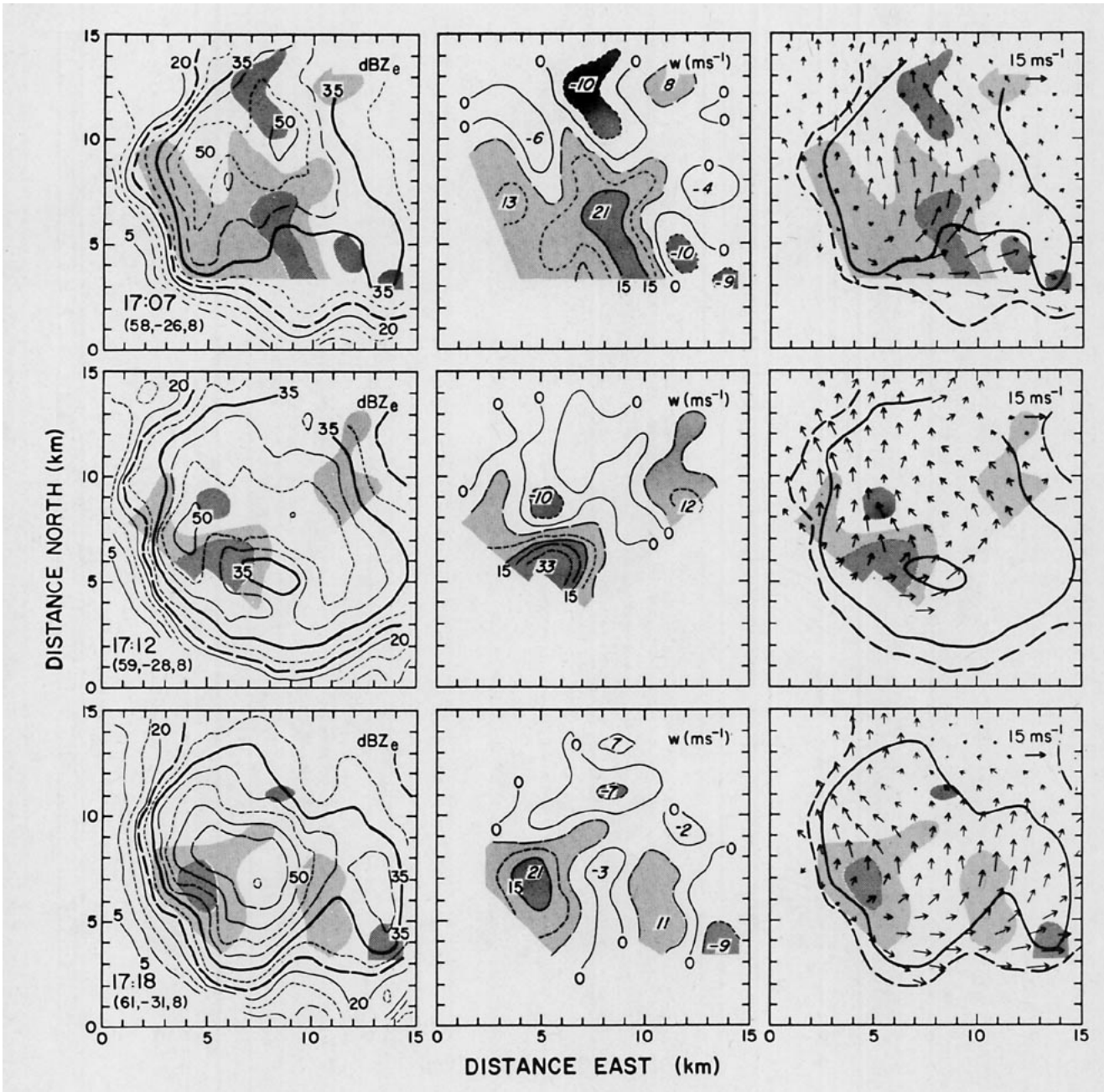

FIG. 17. As in Fig. 16, but at 8 km height.

drafts could be quite significant since if properly positioned they can act as sources of hail embryos for growth in the large updraft.

6. Discussion

a. Airflow structure

The early evolution of the Westplains storm, as discussed in Part I, was dominated by the regular appearance on its right flank of new cells that grew to dominate the storm as older cells dissipated. Such a pattern of evolution is typical of what were called "organized multicells" in Part I. During the last hour or so of its lifetime, however, including the period covered here by the Doppler analysis, the large-scale features of the echo pattern did not undergo significant change. During this period the storm had features in common with previous descriptions of supercell storms, including a quasi-steady reflectivity structure with a pronounced forward overhang, a persistent updraft at cloud base, and weak echo vaults (though the vaults were transient in the present case). It has been shown here, particularly for the 1626–

1640 period, that in certain aspects the airflow from the triple-Doppler measurements was quite similar to the supercell model of Browning and Foote (1976), and this may be taken as a verification that the general features of the airflow for that model are, in fact, characteristic of certain types of storms.

Fig. 18 shows a synthesis of the storm-scale airflow for the present storm based on Doppler, surface, and aircraft measurements. The dominant feature of the circulation is the large updraft, labeled A in the figure, that originates in the low levels from the south-southeast, rises abruptly as it is lifted over a surface gust front and passes through cloud base, and finally turns back in the direction of the storm-relative winds in the upper troposphere to form the anvil streaming away toward the northeast. The cyclonic twist depicted in the updraft ribbon in Fig. 18 is meant to illustrate qualitatively the cyclonic vorticity in the updraft. While the updraft itself possesses cyclonic rotation, individual streamlines (for example, the edges of the updraft ribbon shown) actually turn anticyclonically, as discussed in Section 4.

On the shoulders of the updraft the horizontal momentum is similar to that in the updraft core, while of course the updraft strength is reduced. The streamlines shown alongside the broad updraft, labeled B, are tilted more toward the back of the storm and eventually enter the lower part of the anvil. For purposes of clarity we have not attempted to indicate the presence of smaller updrafts peripheral to the major updraft in Fig. 18. However, as noted in the previous sections, they seem to be commonly present and are probably very significant in terms of microphysical processes in the storm.

In the middle levels the environmental flow is from the west, and is to an extent forced to flow around the storm as if it were a solid barrier (streamlines labeled C). As a barrier, the storm is, in fact, rather porous, and streamlines such as D and E represent air entering the storm on its upwind flank much as packets of chaff have been observed to enter a storm's radar echo (Fankhouser, 1971). Flow along the cyclonic streamline D is substantially stronger than that along E, a result that is apparently general for right-moving storms. As D passes around the east side of the updraft it turns downward to form a principal branch of the storm downdraft and surface outflow, similar to Browning's (1964) depiction. During the period 1626–1640, streamline E was also observed to contribute to a downdraft in the vicinity of the echo core, just north of the updraft. However, in the 1707–1718 Doppler analyses this branch of the flow was not present, and the downdraft in that region was fed partly by air that had traveled along a path initially

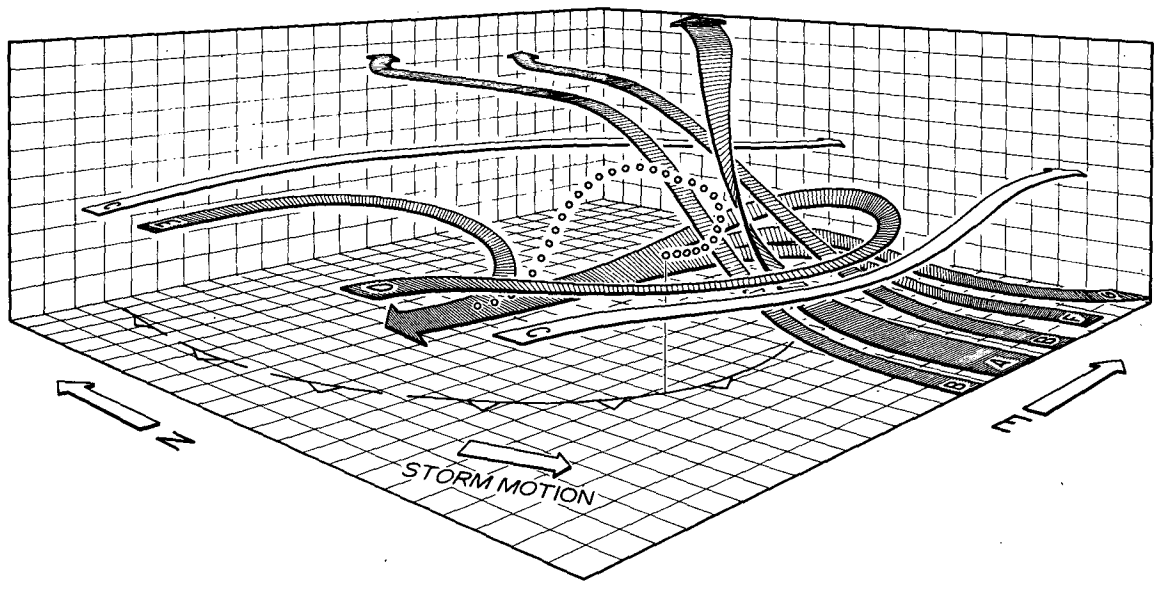

FIG. 18. Major components of the airflow in the Westplains storm. The strong updraft is depicted by the ribbon labeled A, which starts in the low levels to the south-southeast of the storm, rises sharply in the storm interior, and leaves the storm toward the northeast to form the anvil outflow. On the flanks of the strong updraft the air rises more slowly and penetrates farther to the rear of the storm before also turning to the northeast. In the middle levels there is a tendency for the westerly environmental flow to be diverted around the sides of the storm (streamlines labeled C) but some air also enters the storm (streamlines D and E) and contributes to the downdraft. A contribution to the downdraft flux is also made by air originally in the low levels to the southeast and east of the storm (streamlines F and G), which then rises several kilometers before turning downward in the vicinity of the echo core. The various streamlines are depicted relative to the storm, which is moving toward the south-southeast as shown, rather than relative to the ground. The small circles indicate the possible trajectory of a hailstone.

like D, but extending around the storm to its north side. Part of the northern downdraft at both times also originated with air initially rising on the northern side of the updraft. This air can be traced backward along streamline F, shown in Fig. 18, to a source in the low-level environment to the southeast of the Westplains storm. The surface measurements reported by Wade and Foote (1982) indicate that this air was too dry to be convectively unstable. Some of the downdraft air may have originated in the low-level outflow from an adjacent storm just to the east, as depicted by streamline G. The circulation along streamlines F and G is qualitatively similar to that proposed in the original supercell model of Browning and Ludlam (1962). Though the downdraft air near the surface is shown in Fig. 18 as moving primarily toward the west, there is in fact some spreading of the cold downdraft in all directions as it encounters the earth's surface. The position of the cold air boundary is noted in the figure.

From the point of view of understanding hail growth, the processes occurring along paths A and D in Fig. 18 are the most important. The liquid water contained in the supercooled droplets carried by the updraft along path A provides suitable conditions for hail growth, while paths such as D provide a mechanism for transporting potential hail embryos to the west, south, and east sides of the updraft periphery. It is this aspect of the airflow that was first emphasized in the supercell model of Browning and Foote (1976) with reference to hail formation. The dots in the figure show a possible trajectory of a hailstone growing in this way. Heymsfield *et al.* (1980) discuss other examples.

b. Storm models and the evolution continuum

There seems to be some agreement that multicell and supercell models of storms represent well only a fraction of the population of storms, and that a continuum of storm types probably exists, perhaps with these two models as extremes (e.g., WMO, 1981). If cell lifetime is thought of as the principal distinguishing characteristic (Browning, 1977), then a continuum in terms of cell lifetime can be easily visualized. However, there are also structural characteristics of storms that are important in a classification scheme, and results from the present study provide some clues as to how these might change as one moves along a continuum of storm types.

While the present storm had attributes of previous supercell models as described above, it also had certain features such as periodic echo intensifications that were reminiscent of multicell behavior. In terms of its evolution, the characteristics of the present storm were, in fact, intermediate in a sense between these two extremes. This is illustrated in Fig. 19. In the left panel the evolution of the updraft of two cells of a multicell storm is depicted. In the multicell model described by Browning *et al.* (1976) the young updraft is thought of as being a discrete, closed system. As it grows to dominate and in fact to become the mature storm, the older updraft dissipates. In the supercell case shown in the right panel the updraft is quasi-steady. It may have some minor evolution in its upper part, as sketched in the figure (separate radar tops can often be identified in supercell storms, for example; Chisholm (1973), Nelson and Braham (1975) and Foote and Mohr (1979) have discussed certain variations in the geometry of the echo-weak vault), but basically the updraft is thought of as being steady in the middle region most important for precipitation.

In the evolution deduced for the present storm, shown in the middle panel of Fig. 19, the new updraft is neither wholly discrete nor wholly steady, but is somewhere in between. A new updraft surge originates in the lower region of the cloud, and grows in such a way as to produce a modulation of the existing updraft in the manner illustrated, rather than a separate entity. Following the discussion in Part I, we call this "weak evolution" in contrast to the "strong evolution" of the multicell model.

For the purpose of describing such an evolution continuum, it is the distance l between successive large updrafts that is the appropriate variable. When l is greater than the updraft diameter D one has the multicell case. When l is very small, $l \ll D$, one has the supercell model. When l is in between, one has the case of weak evolution.

The illustration in Fig. 19 for the Westplains storm represents one type of storm evolution that differs from the two classical models. In fact, if a wide spectrum of storm behavior is to be considered, it may prove useful to generalize the concept of weak evolution from this specific example. We suggest that the term be applied to all situations in which a discrete storm updraft evolves by undergoing only gradual changes in structure over a period longer than a nominal cell lifetime (15–20 min). Thus, as an alternative example, the merger of a weak cumulus tower with a large storm updraft might serve to perturb the mature updraft, and perhaps even intensify it as suggested by Lemon (1976b). However, in the sense that this evolution is not characterized by the growth of a new intense updraft and the dissipation of an old one, but rather by the persistence of a single large updraft (albeit slightly modified), it could be considered a type of weak evolution.

These ideas imply that attempts to distinguish separate cells during the history of a weakly evolving storm system will entail a much greater degree of arbitrariness than is the case with strongly evolving systems. While strong evolution implies discrete propagation, weak evolution implies propagation that is intermediate between the strictly continuous propagation of the classical supercell case, and the discrete

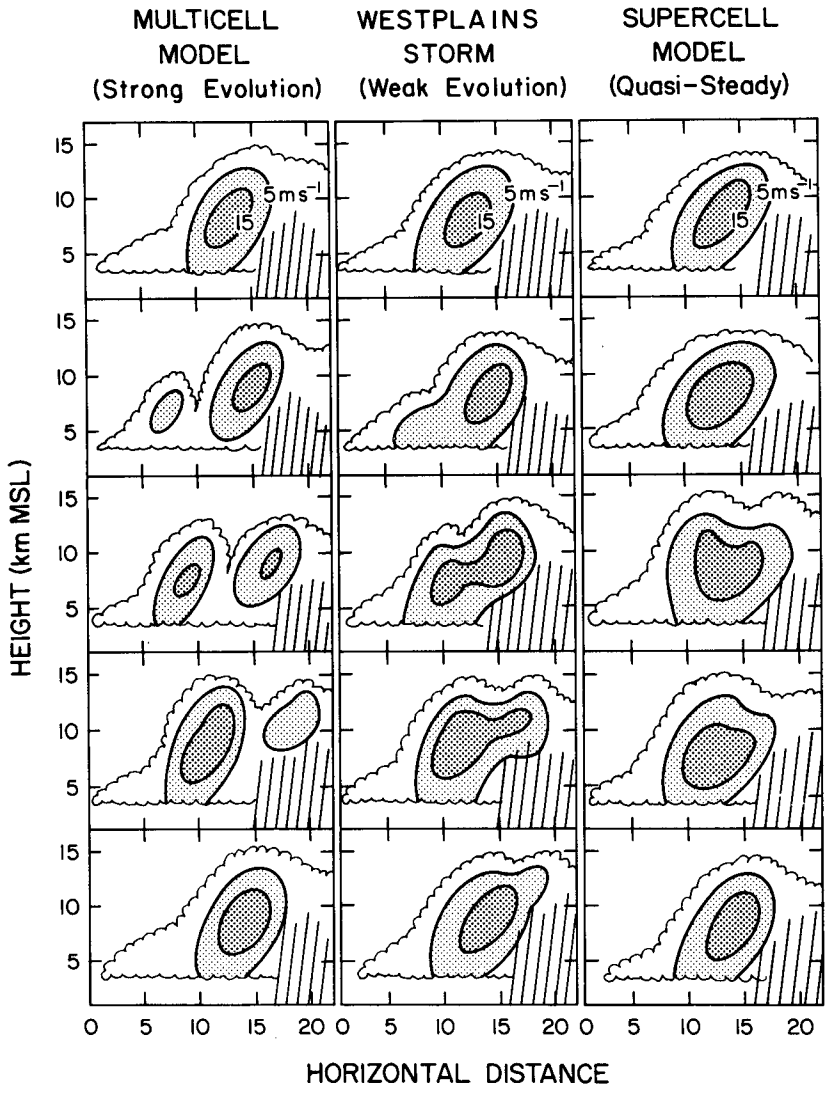

FIG. 19. Schematic diagram showing the updraft evolution for three different storm models. The contours represent isotachs of vertical wind speed. The left panel depicts the cellular evolution according to the multicell model, involving the formation of discrete updrafts. In the supercell model, on the right, the updraft is shown as being quasi-steady. In the model deduced for the Westplains storm, shown in the middle, the large updraft undergoes gradual changes but remains singly connected. This is termed weak evolution, in contrast to the strong evolution of the multicell case. The time between successive frames, moving down the figure, is meant to be 3–5 min.

propagation of the multicell case. Many storms that have been called supercells in the literature appear, upon reexamination, to have undergone some sort of weak evolution as part of their normal course of events (e.g., Lemon, 1976b). Similarly, as mentioned in Part I, the evolution of the Raymer storms described by Browning *et al.* (1976) and others was probably much closer to the weak-evolution model than the multicell model originally ascribed to it. We conclude that while the generality of the present model is not known, the evolution of many storms will prove to fit better the model of weak evolution than the multicell or supercell model.

7. Summary

Triple-Doppler measurements have been analyzed for six periods of time to deduce the airflow in the Westplains storm, a hailstorm of moderate intensity over the High Plains of northeastern Colorado. The horizontal wind fields showed a marked similarity at each of the times, with characteristics that are now

commonly reported: tendency for the updraft to act as a barrier to the environmental flow in the mid-levels, for the momentum in the strong updraft to reflect that in the low-level inflow, and for strong divergence to be the prominent feature aloft. The vertical motion field was dominated at all times by a single large updraft of magnitude 25–30 m s^{-1}. Smaller updrafts tended to be found around its periphery. The persistence and organization of the large updraft with respect to the cyclonic branch of the barrier flow was the same as that proposed in the supercell model of Browning and Foote (1976), with important consequences for the growth of hail as discussed by these authors. The downdraft structure synthesized for the storm had aspects in common with the different models of Browning (1964) and Browning and Ludlam (1962). The downdraft air apparently originated over a broad layer from the mid levels to the surface.

Though the large updraft was persistent, it was possible, with the aid of the reflectivity analysis from Part I, to deduce a pattern of updraft evolution that led to periodic echo intensification. This pattern, termed weak evolution, involves gradual changes in the structure of a long-lived updraft. It leads to a storm model that is intermediate in a certain sense between the classical multicell and supercell descriptions. It now seems probable that many storms that have been previously classified in one of the latter two categories will actually fit the model of weak evolution better.

Acknowledgments. The measurements were collected by the staff of the Wave Propagation Laboratory, NOAA, and the Field Observing Facility, NCAR, whose efforts in this regard are greatly appreciated. L. Jay Miller was particularly instrumental in organizing the field effort and supervising software development.

REFERENCES

Barnes, S. L., 1978: Oklahoma thunderstorms on 29–30 April 1970: Part I. Morphology of a tornadic storm. *Mon. Wea. Rev.*, **106,** 673–684.

Battan, L. J., 1980: Observations of two Colorado thunderstorms by means of a zenith-pointing Doppler radar. *J. Appl. Meteor.*, **19,** 580–592.

Brandes, E. A., 1978: Mesocyclone evolution and tornadogenesis: some observations. *Mon. Wea. Rev.*, **106,** 995–1011.

——, 1981: Fine structure of the Del City–Edmond tornadic mesocirculation. *Mon. Wea. Rev.*, **109,** 635–647.

Browning, K. A., 1964: Airflow and precipitation trajectories within severe local storms which travel to the right of the winds. *J. Atmos. Sci.*, **21,** 634–639.

——, 1977: *The Structure and Mechanisms of Hailstorms. Hail: A Review of Hail Science and Hail Suppression, Meteor. Monogr.*, No. 38, Amer. Meteor. Soc., 1–43.

——, J. C. Fankhauser, J-P. Chalon, P. J. Eccles, R. G. Strauch, F. H. Merrem, D. J. Musil, E. L. May and W. R. Sand, 1976: Structure of an evolving hailstorm, Part V: Synthesis and implications for hail growth and hail suppression. *Mon. Wea. Rev.*, **104,** 603–610.

——, and G. B. Foote, 1976: Airflow and hail growth in supercell storms and some implications for hail suppression. *Quart. J. Roy. Meteor. Soc.*, **102,** 499–533.

——, and F. H. Ludlam, 1962: Airflow in convective storms. *Quart. J. Roy. Meteor. Soc.*, **88,** 117–135.

Chisholm, A. J., 1973: *Alberta Hailstorms:* Part I. Radar studies and airflow models. *Meteor. Monogr.*, No. 36, Amer. Meteor. Soc., 1–36.

Eagleman, J. R., and W. C. Lin, 1977: Severe thunderstorm internal structure from dual-Doppler radar measurements. *J. Appl. Meteor.*, **16,** 1036–1048.

Fankhauser, J. C., 1971: Thunderstorm-environment interactions determined from aircraft and radar observations. *Mon. Wea. Rev.*, **99,** 171–192.

Foote, G. B., and J. C. Fankhauser, 1973: Airflow and moisture budget beneath a northeast Colorado hailstorm. *J. Appl. Meteor.*, **12,** 1330–1353.

——, and C. G. Mohr, 1979: Results of a randomized hail suppression experiment in northeast Colorado. Part VI: Post hoc stratification by storm intensity and type. *J. Appl. Meteor.*, **18,** 1589–1600.

——, and C. G. Wade, 1982: Case study of a hailstorm in Colorado. Part I: Radar echo structure and evolution. *J. Atmos. Sci.*, **39,** 2828–2846.

Frank, H. W., and G. B. Foote, 1982: The 22 July 1976 case study: Storm airflow, updraft structure, and mass flux from triple-Doppler measurements. *Hailstorms of the Central High Plains,* Vol. 2, Colorado Associated University Press, 131–162.

Heymsfield, A. J., and D. J. Musil, 1982: Case study of a hailstorm in Colorado. Part II: Particle growth processes at the mid-levels as deduced from the *in situ* measurements. *J. Atmos. Sci.*, **39,** 2847–2866.

——, A. R. Jameson and H. W. Frank, 1980: Hail growth mechanisms in a Colorado storm: Part II. Hail formation processes. *J. Atmos. Sci.*, **37,** 1779–1807.

Heymsfield, G. M., 1978: Kinematic and dynamic aspects of the Harrah tornadic storm analyzed from dual-Doppler radar data. *Mon. Wea. Rev.*, **106,** 233–254.

——, 1981: Evolution of downdrafts and rotation in an Illinois thunderstorm. *Mon. Wea. Rev.*, **109,** 1969–1988.

Klemp, J. B., R. B. Wilhelmson, and P. S. Ray, 1981: Observed and numerically simulated structure of a mature supercell thunderstorm. *J. Atmos. Sci.*, **38,** 1558–1580.

Kohn, N. M., A. L. Johnston and C. Mohr, 1978: MUDRAS: Multiple Doppler radar analysis system. NOAA Tech. Memo. No. ERL WPL-35, Wave Propagation Laboratory, Boulder, 168 pp.

Kropfli, R. A., and L. J. Miller, 1976: Kinematic structure and flux quantities in a convective storm from dual-Doppler radar observations. *J. Atmos. Sci.*, **33,** 520–529.

Lemon, L. R., 1976a: Wake vortex structure and aerodynamic origin in severe thunderstorms. *J. Atmos. Sci.*, **33,** 678–685.

——, 1976b: The flanking line, a severe thunderstorm intensification source. *J. Atmos. Sci.*, **33,** 686–694.

——, and C. A. Doswell III, 1979: Severe thunderstorm evolution and mesocyclone structure as related to tornadogenesis. *Mon. Wea. Rev.*, **107,** 1184–1197.

Lhermitte, R. M., and M. Gilet, 1975: Dual-Doppler radar observation and study of sea breeze convective storm development. *J. Appl. Meteor.*, **14,** 1346–1361.

Marwitz, J. D., 1972a: The structure and motion of severe hailstorms: Part I. Supercell storms. *J. Appl. Meteor.*, **11,** 166–179.

——, 1972b: The structure and motion of severe hailstorms: Part II. Multi-cell storms. *J. Appl. Meteor.*, **11,** 180–188.

Miller, L. J., 1975: Internal airflow of a convective storm from dual-Doppler radar measurements. *Pure Appl. Geophys.*, **113,** 765–785.

Moncrieff, M. W., and M. J. Miller, 1976: The dynamics and sim-

ulation of tropical cumulonimbus squall lines. *Quart. J. Roy. Meteor. Soc.*, **102,** 373–394.

Nelson, S. P., and R. R. Braham, Jr., 1975: Detailed observational study of a weak echo region. *Pure Appl. Geophys.*, **113,** 735–746.

Ray, P. S., 1976: Vorticity and divergence fields within tornadic storms from dual-Doppler radar observations. *J. Appl. Meteor.*, **15,** 879–890.

——, B. C. Johnson, K. W. Johnson, J. S. Bradberry, J. J. Stephens, K. K. Wagner, R. B. Wilhelmson and J. B. Klemp, 1981: The morphology of several tornadic storms on 20 May 1977. *J. Atmos. Sci.*, **38,** 1643–1663.

Rotunno, R., 1981: On the evolution of thunderstorm rotation. *Mon. Wea. Rev.*, **109,** 577–586.

Schlesinger, R. E., 1978: A three-dimensional numerical model of an isolated thunderstorm: Part I. Comparative experiments for variable ambient wind shear. *J. Atmos. Sci.*, **35,** 690–713.

——, 1980: A three-dimensional numerical model of an isolated thunderstorm: Part II. Dynamics of updraft splitting and mesovortex evolution. *J. Atmos. Sci.*, **37,** 395–420.

Wade, C. G., and G. B. Foote, 1982: The 22 July 1976 case study: Low level airflow and mesoscale influences. *Hailstorms of the Central High Plains,* Vol. 2, Colorado Associated University Press, Boulder, 115–130.

Wilhelmson, R. B., and J. B. Klemp, 1981: A three-dimensional numerical simulation of splitting severe storms on 3 April 1964. *J. Atmos. Sci.*, **38,** 1581–1600.

World Meteorological Organization, 1981: The dynamics of hailstorms and related uncertainties of hail suppression. *Hail-Suppression Research Report,* No. 3, WMO, Geneva, 22 pp.